RSC Advances

Controllable synthesis, Photocatalytic and Electrocatalytic Properties of CeO2 Nanocrystals

Journal:	*RSC Advances*
Manuscript ID:	RA-ART-04-2015-006213
Article Type:	Paper
Date Submitted by the Author:	19-Apr-2015
Complete List of Authors:	Li, Li; Nanjing University of Science and Technology, Wang, Haoran; Nanjing University of Science and Technology, Zou, Lei; Nanjing University of Science and Technology, Wang, Xiong; Nanjing University of Science and Technology, School of Materials Science and Engineering

Cite this: DOI: 10.1039/c0xx00000x

www.rsc.org/xxxxxx

ARTICLE TYPE

Controllable synthesis, Photocatalytic and Electrocatalytic Properties of CeO_2 Nanocrystals

Li Li,[a,b] Haoran Wang, [a] Lei Zou [a] and Xiong Wang*[a, c]

Received (in XXX, XXX) Xth XXXXXXXXX 20XX, Accepted Xth XXXXXXXXX 20XX

DOI: 10.1039/b000000x

Uniform CeO_2 nanoparticles and nanorods were selectively synthesized through a hydrothermal method followed by calcination. UV-vis diffuse reflection spectra (DRS) exhibited that the obtained powders were responsive to visible light, which might be attributed to the presence of increased oxygen vacancies in the ceria structure. The enhanced photocatalytic activities of CeO_2 nanostructures were comparatively evaluated by the photodegradation of rhodamine B under visible light, far exceeding that of the commercial P25 powders. The mechanism was investigated through the carriers trapping experiments. Meanwhile, the glass carbon electrode (GCE) decorated with the resulting nanocrystals was used to examine the electrocatalytic behavior for *p*-nitrophenol degradation in a basic solution. The results demonstrated substantially the obtained CeO_2 nanoparticles with excellent photocatalytic and electrocatalytic activities.

Introduction

Nanostructured functional materials have attracted much research interest due to excellent physical and chemical properties depending on their size, shape, or surface, et al.[1–4] CeO_2 is a typical kind of important and relatively harmless rare earth oxide due to its inherent properties, including oxygen ion conductivity, oxygen storage capacity, catalysis, optics, magnetics, and high chemical and thermal stability.[5–8] So it has significant and fascinating applications in a wide variety of fields such as catalysis, absorbents, solid oxide fuel calls (SOFC), hydrogen storage materials, and separation.[9–11]

Currently, a variety of chemical techniques have been utilized to prepare ceria nanocrystals (NCs), including sol-gel method,[12] precipitation,[13] microemulsion process,[14] sonochemical method,[12] glycine-nitrate combustion,[15] surfactant template synthesis,[16, 17] and so on.[18–20] The hydro/solvothermal method is one of most important approaches for the preparation of novel nanostructures.[21, 22] In particular polyol-mediated (e.g. ethylene glycol, triethylene glycol, tetraethylene glycol and glycerol) reaction media have been widely used in solvothermal process due to their special physical and chemical properties such as the strong chelating ability of hydrogen bonds between hydroxyl groups, which facilitates the formation of complexes with metal ions.[23, 24] However, most of these preparation techniques are energy-consuming and manufacture-complicated. And there have been very few reports on its photocatalytic and electrocatalytic behaviors.

Herein, we presented a versatile hydrothermal route followed by calcination to selectively prepare CeO_2 nanoparticles (NPs) and nanorods (NRs). Rhodamine B (RhB), as a typical environmental contaminant, is generally considered to be very stable to light and difficult to be decomposed under solar light. It has been widely used for investigating the photocatalytic activity of various types of photocatalysts. According to the results of RhB photodegradation experiments, a photocatalytic mechanism was also proposed. Moreover, phenol and its derivants are indentified as great threats to the environment and even their contamination in water at a low concentration is highly carcinogenic to human beings and animals.[25] Recently, considerable attention has been paid to chemical degradation of phenol and its derivants.[26, 27] In the work, we attempted to degrade *p*-nitrophenol existing in a basic solution via an electrocatalytic redox process using the as-prepared CeO_2 samples as catalyst.

Experimental

Synthesis of CeO_2 nanostructures

All chemicals are reagent grade and used without further purification. In a typical synthesis of ceria NPs, 5 mmol $Ce(NO_3)_3 \cdot 6H_2O$ was dissolved in 20 mL absolute alcohol to form homogeneous solution. Then, 40 mL 0.4 mol·L^{-1} NaOH ethanol solution was dropwise dripped into the above solution and stirred magnetically for 30 min. Subsequently, the mixture was transferred into a Teflon-lined autoclave, sealed and heated at 120 °C for 12 h. After the hydrothermal treatment, the precipitate were collected by centrifugation, washed several times with deionized (DI) water and absolute ethanol to remove possible residues, and followed by drying in an oven at 80 °C. Finally, the NPs were obtained after calcination in ambient air at 300 °C for 2 h. For the NRs, the similar procedure was conducted just replacing absolute alcohol with DI water as solvent. The rest of the synthetic procedure was similar to that used for the synthesis

of the NPs.

Characterization

The phases of the samples were examined by X-ray diffraction (XRD) on a Bruker D8 Advanced diffractometer. The patterns were collected using unfiltered Cu K_α-radiation and the Bragg–Brentano geometry over the 2θ range 10–80°. The morphology of the as-prepared sample was observed by transmission electron microscopy (TEM, Hitachi, Model H-800, accelerating voltage 200 kV). UV–vis diffuse reflection spectroscopy (DRS) of the samples was conducted on a Shimadzu UV2450 UV–vis spectrophotometer equipped with an integrating sphere. The specific surface areas of the samples were measured by a V-sorb 2800 Brunauer–Emmett–Teller specific surface area instrument. The photoluminescence (PL) spectra of photocatalysts were detected on a Hitachi F4600 type spectrometer with excitation wavelength of 203 nm.

Photocatalytic test

The photocatalytic activities of CeO_2 NCs were evaluated by the photodegradation of rhodamine B (RhB) under visible light irradiation. The visible-light source was a 500 W Xe lamp positioned in a quartz cold trap which was in the middle of multiposition cylindrical reaction vessel. The system was cooled by wind and water and was maintained at the room temperature. Appropriate cut-off filters were placed around the cold trap to completely remove of radiation below 420 nm ensuring that the catalysis of the RhB/CeO_2 system occurred only under visible light.

In the experiment, 20 mg CeO_2 were added to 20 mL RhB solution (10^{-5} mol L^{-1}) in a reaction vessel. Before illumination, the suspensions were stirred in the dark for 30 min to ensure the establishment of an adsorption–desorption equilibrium between the photocatalyst and RhB. Then the solution was exposed to visible light irradiation under stirring. At given time intervals, a small quantity of suspension was sampled and centrifuged to remove the photocatalyst particles. The supernatants were analyzed by measuring the absorption spectrum using the UV–vis spectrophotometer. The commercial TiO_2 (Degussa P25) powders were adopted as the reference to compare the photocatalytic activity under the same experimental processes and conditions.

Electrochemical property measurement

The electrocatalytic degradation of *p*-nitrophenol (PNP) in basic solution was performed on a CHI760D microcomputer-based electrochemical system (Shanghai Chenhua Instrument Co., Ltd, China). A three-electrode single compartment cell was used for cyclic voltammetry with sodium hydroxide (1.0 mol L^{-1}) and PNP (1.0 mol L^{-1}) as electrolyte. A glassy carbon electrode (GCE, 2.0mm diameter) was used as the working electrode, a platinum plate as the counter electrode, and an Ag/AgC1 electrode as the reference electrode. Prior to each measurement, the GC electrode surface was carefully polished on an abrasive paper, then further polished with 1.0, 0.3 and 0.05 μm α-Al_2O_3 (Buehler) paste in turn, and thoroughly rinsed successively with 3 mol L^{-1} H_2SO_4 aqueous solution, doubly distilled water, and acetone, and finally dried in the air. A total of 5 mg of CeO_2 sample was dispersed in 1 mL doubly distilled water under an ultrasonic treatment to obtain a yellow suspension solution. A drop of the solution was trickled with a syringe onto the carbon surface of the GC electrode. After being dried in the air, the modified GC electrode was successfully prepared and used directly for electrochemical measurements.

Results and discussion

XRD analysis was carried out to investigate the phase and purity of the as-synthesized samples. The typical XRD patterns of CeO_2 are shown in Fig. 1. All the reflection peaks can be indexed to the face-centred cubic (*fcc*) structure of CeO_2 (space group: $Fm\bar{3}m$[225]), which is in good agreement with the standard data reported in JCPDS Card (No.34-0394). The XRD results reveal that the samples are highly crystallized and exhibit a single-phase structure. It is noted that the pure-phase CeO_2 could be obtained whether the solvent is ethanol or DI water. The average crystallite size of the NPs is about 7.5 nm calculated from Scherer's formula.

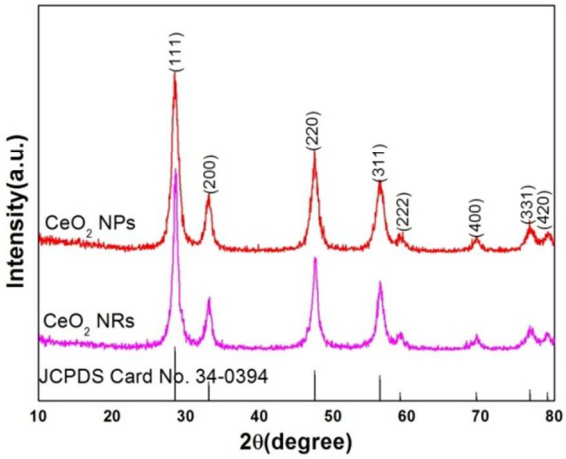

Fig. 1. XRD patterns of the obtained CeO_2 powders.

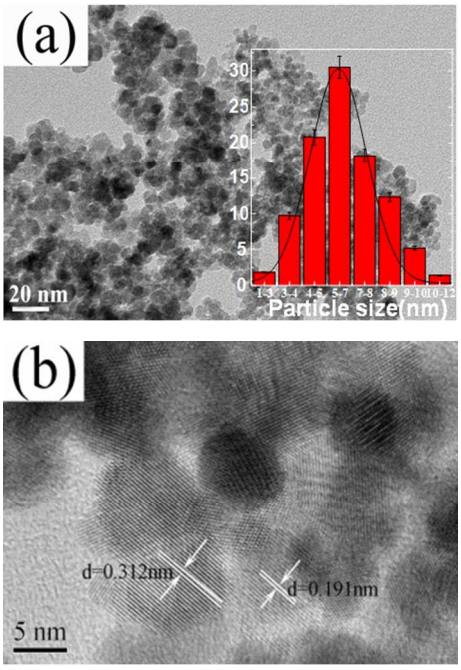

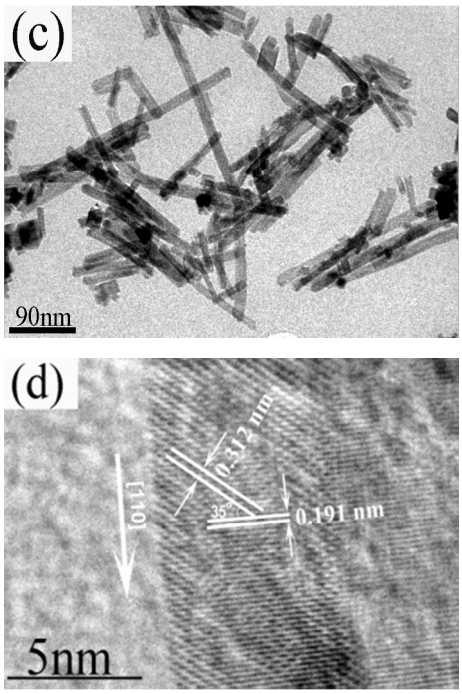

Fig. 2. TEM and HRTEM images of (a, b) CeO_2 NPs and (c, d) CeO_2 NRs, respectively. Inset: Histogram of size distribution for CeO_2 NPs.

The morphologies of the samples were observed by TEM, which are shown in Fig. 2. From Fig. 2a, it was observed that the resulting NPs are uniform in shape and size, and the average diameter of particles in the range of 3-10 nm with a narrow size distribution, which was consistent with the XRD result. Two interplanar spacings of the ordered stripes marked in Fig. 2b were 0.312 and 0.191 nm, corresponding to (111) and (220) lattice planes of the *fcc* CeO_2, respectively. While the solvent was replaced with DI water, as shown in Fig. 2c, the obtained powders are composed of ceria NRs. Such NRs typically have diameters of around 13 nm and lengths up to 80-200 nm. Fig. 2d shows the clear lattice fringes of (111) and (220) with interplanar spacings of 0.312 and 0.191 nm respectively, and the interfacial angle between the (111) and (220) facets is about 35° indicating the cubic structure of CeO_2 NRs with [110] growth direction.

Fig. 3 reveals the diffuse reflection spectra of the synthesized CeO_2 NCs. In contrast to P25 whose absorption edge was about 400 nm, both the ceria samples exhibited extremely clear absorption in UV–vis light region. Band gap determines what portion of the solar spectrum a photocatalyst absorbs. Depending on the Kubelka–Munk formula, the relationship between the optical absorption coefficient of an indirect gap semiconductor and the band-gap energy follows the Tauc's relation: $(\alpha h\nu)^{1/2} = B(h\nu - E_g)$, where α, h, ν, E_g and B is absorption coefficient, Planck constant, light frequency, band gap, and a constant, respectively. From the equation $(\alpha h\nu)^{1/2}$ has a linear relation with $h\nu$. Extrapolating the linear relation as $(\alpha h\nu)^{1/2} = 0$ gives the band-gap E_g of approximately 2.60, 2.65 eV for CeO_2 NRs and NPs as shown in Fig. 3b, slightly lower than literatures,[28, 29] which might be attributed to the presence of increased oxygen vacancies in the ceria NCs, leading to a distortion of the local symmetry.[30, 31] As compared with the NRs, the band gap of the NPs was increased by 0.05 eV, indicating the existence of a quantum confinement effect. Some previous studies also reported the quantum size effects in nanostructured CeO_2 systems. From the Tuac plot, the band gap of commercial P25 was also estimated to be 3.07 eV.

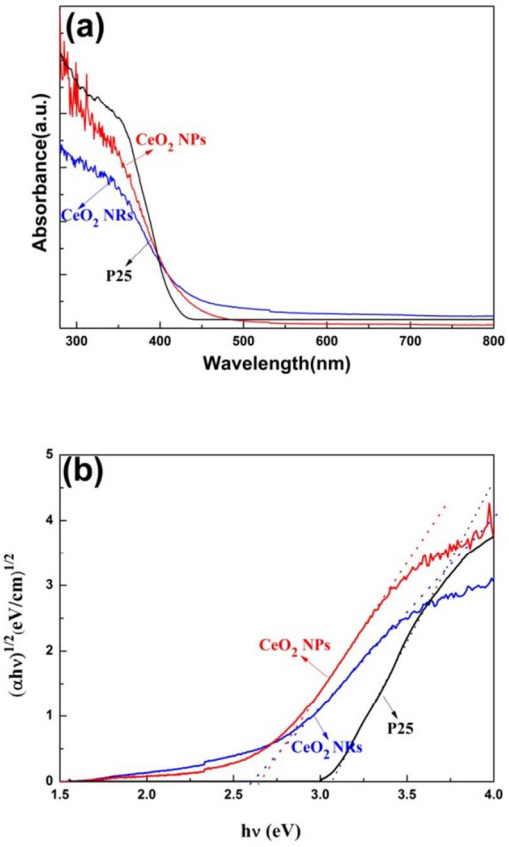

Fig. 3. (a) Diffuse reflection spectra of CeO_2 NPs, CeO_2 NRs, and P25. (b) The corresponding $(\alpha h\nu)^{1/2}$–$h\nu$ plots.

Fig. 4a shows the temporal changes of the absorption spectrum of RhB solution during the photodegradation process of CeO_2 NPs. According to Beer-Lambert law $A=kbc$, it can be concluded that approximately 83% of RhB was photodecomposed after illumination for 240 min. There are no changes in the characteristic peak shape and vertical position except the peak intensity, which indicates that the predominant degradation mechanism of RhB is a hydroxylation/oxidation process.[32] When the presence of light energy is equal to or greater than the bandgap of CeO_2, the electrons receive the energy and transfer of electrons from valence band (VB) to conduction band (CB) which results in the formation of a hole (h^+) in the VB and an electron (e^-) in the CB. The holes react with water and generate •OH, which can oxidize the organic pollutants. In the conduction band the electrons react with oxygen and undergo reduction process and produce •OH. These radicals can reduce the organic pollutants. This oxidation and reduction processes were capable of degrading the RhB under visible light irradiation.

Furthermore, the photocatalytic degradation kinetics of RhB over CeO_2 NPs/NRs under visible light irradiation were determined using the Langmuir-Hinshelwood model, which can be simplified as a pseudo first-order reaction as follows:[33] where C is the RhB concentration at the time t; C_0 is the initial RhB

concentration measured after the adsorption–desorption equilibrium, k refers to the reaction rate kinetic constant.

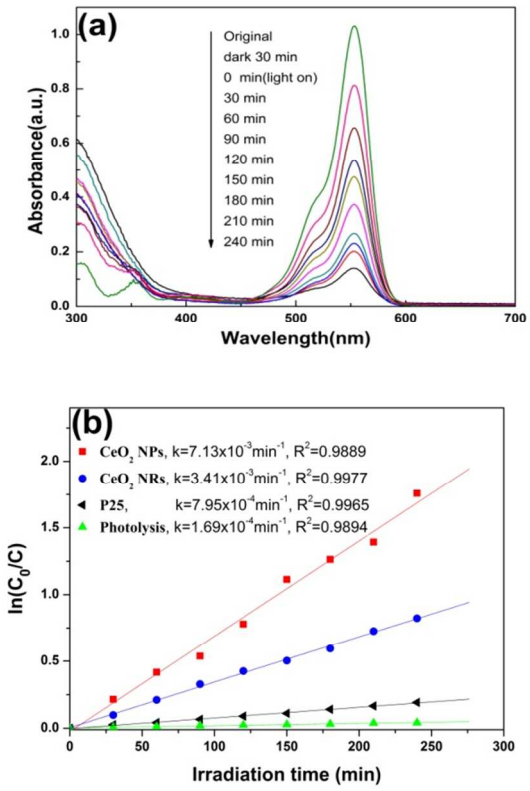

Fig. 4. (a) Absorption changes of RhB solution in visible-light-induced photocatalytic process for CeO_2 NPs. (b) The corresponding photocatalytic kinetics.

As shown in Fig. 4b, a linear relationship is observed between $ln(C_0/C)$ and the reaction time t, and the k values can provide a good evaluation on the overall photocatalytic degradation rates of RhB. Obviously, both the ceria samples exhibited superior photoactivity to P25. The result also shows that the k of 0.0071 min^{-1} for CeO_2 NPs is much higher than that of NRs (0.0034 min^{-1}), indicating the photocatalytic activity of NPs was enhanced more than 2-fold. It may be attributed to the relatively smaller size and larger specific surface area (104.7 *vs.* 36.8 m^2 g^{-1}), which is considered to favourably reduce the chance of the recombination between photogenerated hole and electron inside the crystal,[34, 35] so that more photogenerated charge carriers can transfer to the photocatalyst surface. Meanwhile, the larger band gap produced by shifting CB and VB in opposite directions usually tends to increase the surface redox potential and prolong the carrier lifetime. All of these endow the CeO_2 NPs with more excellent photocatalytic performances. As a whole, the primary factor responsible for the enhanced visible light photoactivity of CeO_2 NPs is the band gap narrowing effect of the oxygen excess defect.

Photoluminescence (PL) analysis could be applied to reveal the efficiency of charge carrier trapping and separation of the photoinduced electrons and holes in semiconductor. Fig. 5 shows the room temperature PL spectra of the CeO_2 nanostructures. Several emission peaks centered at ~439 (2.82 eV), 452 (2.74 eV), 469 (2.64 eV), 482 (2.57 eV), 492 (2.52 eV), 526 (2.36 eV), and 569 nm (2.18 eV) are observed. The broad blue band at 439 nm originates from charge transitions from the 4f band to the valence band of the CeO_2 NCs. The blue (452, 469 nm) and weak blue-green emissions (482, 492 nm) are possibly due to surface defects in the CeO_2 powders.[36, 37] The broad green band at 526 nm may be attributed to the oxygen vacancies during the preparation.[38] Though the both PL spectra are similar in the range from 350 to 550 nm, the intensity of the NPs is lower than that of the latter. The result distinctly implies the lower recombination of electron–hole pairs for the NPs, which is consistent with the photocatalytic testing result.

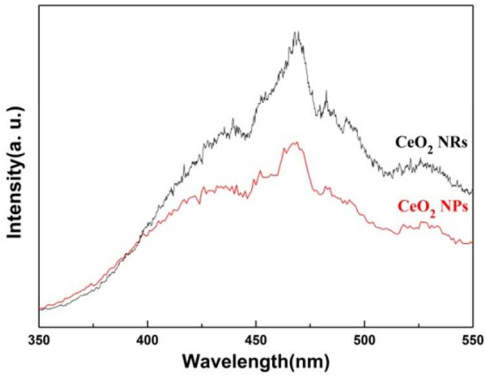

Fig. 5. Room-temperature photoluminescence spectra of CeO_2.

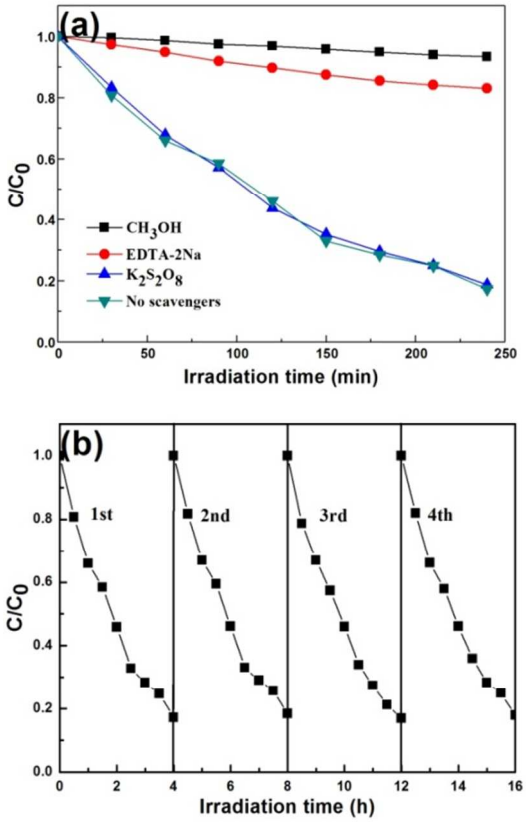

Fig. 6. (a) Photocatalytic degradation of RhB over CeO_2 NPs in the presence of various scavengers. (b) Recycling tests of the NPs under visible light illumination.

Chemical scavengers were employed to investigate the mechanism of the photocatalytic processes and to identify the major contributors to the photocatalytic processes. We also conducted the trapping experiments to determine the main active species during the photocatalysis. Potassium persulfate and disodium ethylenediaminetetraacetate (EDTA-2Na) were used as electrons acceptor and holes scavenger, respectively. As shown in Fig. 6a, the degradation efficiency of RhB is almost no change upon addition of $K_2S_2O_8$. While EDTA-2Na was added, the degradation of RhB decreases to 17%, revealing that the photogenerated holes are the main active species for RhB degradation. Methanol is known to act as a hole scavenger as well as an efficient scavenger of •OH radicals. As shown in Fig. 6a, methanol efficiently suppressed the RhB photodegradation. Therefore, it confirmed that both the holes (h^+) and reactive oxygen species (•OH or/and •OOH) play the dominant roles in RhB photodegradation over CeO_2 while the holes were the main reactive species by comparing with the induced electrons.

The catalyst's lifetime is an important parameter of the photocatalytic process, so it essential to evaluate the stability of the catalyst for practical application. Therefore, the cycling runs for RhB photodegradation over CeO_2 NPs were performed and the result was displayed in Fig. 6b. It was revealed that the photocatalytic activity of CeO_2 NPs for RhB photodegradation can be effectively retained, without significant loss of activity after four recycling runs.

Besides photocatalysis, the electrocatalytic degradation of phenol and its derivants has also attracted considerable attention. Herein, the electrocatalytic property of the obtained ceria powders was also investigated. Cyclic voltammograms (CV) of the bare GCE and the GCE modified with the CeO_2 NPs and NRs in presence of PNP in a basic solution are shown in Fig. 7.

When a bare GCE was used, there is a peak around −0.98 V *vs.* Ag/AgCl with a current peak value of 36.94 μA in the anodic sweep (as shown in Fig. 7a), which is considered as the oxidation reaction of PNP. This evidence indicates that the reaction is composed of a fast electron transfer process followed by a chemical reaction.[39] The peak current was rather low, which suggested that the GCE exhibited poor electrocatalytic activity. While the ceria NRs-modified GCE exhibits obvious catalytic activity for *p*-nitrophenol degradation. Compared with the bare GCE, the peak current value had a distinct increase from 36.94 to 58.49 μA with peak potential almost no change. As to the NPs, the anode peak current was further increased to 70.32 μA, indicating the enhanced electrocatalytic activity for PNP degradation resulting from the smaller particle size and larger specific surface area, which can generate more reactive sites.

Based on the general mechanism for electrochemical degradation of organic compounds on metal oxide electrode,[40] at the first stage, the adsorbed H_2O molecule was assumed to be discharged on the anode to produce •OH: $CeO_2 + H_2O \rightarrow CeO_2(\bullet OH) + H^+ + e^-$. Then, due to the strong electrophilic character, hydroxyl radical attacked $-NO_2$ group with strong electron-withdrawing effect, leading to its detachment from the aromatic ring. These formed hydroquinone and *p*-benzoquinone compounds continued to be further attacked by •OH resulting in aromatic ring opening to form a variety of carboxylic acids.[41] Eventually, these carboxylic acids were thoroughly oxidized into CO_2 and H_2O.

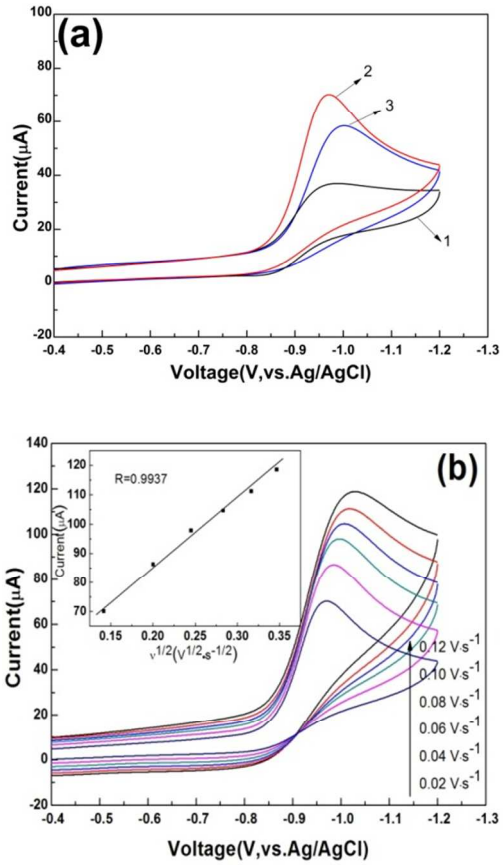

Fig. 7. (a) Cyclic voltammograms (CV) of bare GCE (1), and the GCE modified with CeO_2 NPs (2) and NRs (3) at scanning rate of 0.02 $V \cdot s^{-1}$, respectively. (b) CV curves of the NP-modified GCE at different scanning rates (the insert: the corresponding $I_{pc} \sim v^{1/2}$ plot).

To investigate the effect of scanning rate on the electrocatalytic activity, different rates were tested for the NPs-modified GCE. Fig. 7b shows the cyclic voltammograms of the modified GCE for *p*-nitrophenol degradation at different scanning rates (v). The peak current (I_{pc}) (as shown in the inset of Fig. 7b) increases linearly with the square root of scanning rate ($v^{1/2}$) in the range of 0.02–0.12 $V \cdot s^{-1}$ (the linear dependent coefficient was 0.9937), indicating that the electrocatalytic degradation of *p*-nitrophenol over the GCE/NPs is attributed to diffusion-controlled reaction.[39]

Conclusions

In summary, CeO_2 NPs and NRs were controllably synthesized by a facile hydrothermal method. The visible-light-induced photocatalytic activity was also investigated. The excellent photocatalytic performance of the nanoparticles in visible light region predicts their promising application in water treatment. The trapping experiments of the radicals revealed that the hole was the main reactive species for photocatalytic degradation of RhB and the possible mechanism was proposed. Additionally, the as-prepared CeO_2-decorated GCE was also used to electrocatalytic degradation of PNP. The results indicate that PNP could be degraded with a higher peak current at an invariable peak potential on the GCE modified with the NPs. As a whole,

the obtained CeO_2 NPs presented more excellent visible-light-responsive photocatalytic behavior and higher electrocatalytic activities for PNP degradation in a basic solution.

Acknowledgements

We gratefully acknowledge the financial supports from the NSFC (21001064), the Natural Science Foundation of Jiangsu Province (BK2010487), the key Science Foundation of Huainan Normal University (2014xk10zd), the Key Laboratory of Pollution Control and Resources Reuse of China (PCRRF13014), and the Natural Science Foundation of Anhui Province (1408085QB23). This work was partly sponsored by the CSC.

Notes and references

[a] *School of Materials Science and Engineering, Nanjing University of Science and Technology, Nanjing 210094, China. Fax: +86-25-84313349; Tel: +86-25-84313349; E-mail: xiongwang@njust.edu.cn*
[b] *Department of Chemistry and Chemical Engineering, Huainan Normal University, Huainan 232001, China.*
[c] *Department of Chemistry, Faculty of Science, National University of Singapore, 3 Science Drive 3, 117543, Singapore.*

References:

1 X. H. Lu, D. Z. Zheng, P. Zhang, C. L. Liang, P. Liu and Y. X. Tong, *Chem. Commun.,* 2010, **46,** 7721.
2 Y. Su, Z. Tang, W. Han, P. Zhang, Y. Song and G. Lu, *CrystEngComm*, 2014, **16**, 5189.
3 X. Wang, X. Chen, L. Gao, H. Zheng, Z. Zhang and Y. Qian, *J. Phys. Chem. B*, 2004, 1**08**, 16401; X. Wang, L. Li, Y. Zhang, S. Wang, Z. Zhang, L. Fei and Y. Qian, *Cryst. growth Design* **6 (9)**, 2163.
4 X. Gao, Y. Jiang, Y. Zhong, Z.Y. Luo and K. F. Cen, *J. Hazard. Mater.,* 174 2010, **174,** 734.
5 L. N. Wang and F. M. Meng, *Mater. Res. Bull.,* 2013, **48,** 3492.
6 F. Lu , F. M. Meng , L. N. Wang , J. J. Luo and Y. Sang, *Mater. Lett.*, 2012, **73,** 154.
7 R. K. Singhal, S. Kumar, A. Samariya, M. Dhawana, S. C. Sharma and Y. T. Xing, *Mater. Chem. Phys.,* 2012, **132,** 534.
8 S. Q. Liu, M. J. Xie , X. F. Guo and W. J. Ji, *Mater. Lett.,* 2013, **105,** 192.
9 R. Pérez-Hernández, C. Gutiérrez-Wing, G. Mondragón-Galicia and A. Gutiérrez- Martínez, *Catal. Today,* 2013, **212,** 225.
10 Y. Chen, T. M. Liu, C. L. Chen, W. W. Guo, R. Sun, S. H. Lv, M. Saito, S. Tsukimoto and Z. C.Wang, *Ceram. Int.*, 2013, **39,** 6607.
11 H. Y. Jin , N. Wang , L. Xu and S. E. Hou, *Mater. Lett.,* 2010, **64,** 1254.
12 M. S. Kamal, Khalil, A. Leena, Elkabee and B. Murphy, *Microporous Mesoporous Mater.,* 2005, **78,** 83.
13 N. K. Renuka, *J. Alloys Compd.,* **2012,** 513, 230.
14 P. F. Ji, J. L. Zhang, F. Chen and M. Anpo, *Appl. Catal., B: Enviro.,* 2009, **85,** 148.
15 R. D. Purohit, B. P. Sharma, K. T. Pillai and A. K. Tyagi, *Mater. Res. Bull.,* 2001, **36,** 2711.
16 N. Sabari Arul, D. Mangalaraj, T.W. Kim, P. C. Chen, N. Ponpandian, Meena and Y. Masuda, *J Mater Sci: Mater Electron,* 2013, **24,** 1644.
17 D. Channei, B. Inceesungvorn, N. Wetchakun, S. Phanichphant, A. Nakaruk, P. Koshy and C. C. Sorrell, *Ceram. Int.*, 2013, **39,** 3129.
18 R. Suresh, V. Ponnuswamy and R. Mariappan, *Appl. Surf. Sci.*, 2013, **273,** 457.
19 L. Truffault, C. Andrezza, C. V. Santilli and S. H. Pulcinelli, *Colloid. Surf., A: Physicochem. Eng. Aspects,* 2013, **426,** 63.
20 Z. Ji, X. Wang, H. Zhang, S. Lin, H. Meng, B. Sun, S, George, T. Xia, A. Nel and J. Zink, *ACS Nano*, 2012, **6**, 5366.
21 K. Zhou, Z. Yang, S. Yang, *Chem. Mater.*, 2007, **19**, 1215.
22 N. Sabari Arul, D. Mangalaraj and T. W. Kim, *J Sol-Gel Sci Technol.,* 2013, **66,** 15.
23 D. S. Bae, B. Lim , B. I. Kim and H. Kyong-Sop, *Mater. Lett.,* 2002, **56,** 610.
24 G. Cheng, J. Y. Xiong and F. J. Stadler, *Powder Technol.,* 2013, **249,** 89.
25 M. G. Nickelson, W. J. Cooper, C. N. Kuriez and T. D. Waite, *Environ. Sci. Technol.*, 1992, **26,** 144; L. Li, X. Wang and Y. G. Zhang, *Mater. Res. Bull.*, 2014, **50**, 18.
26 D. H. Bremner, A. E. Burgess, D. Houllemare and K.C. Namkung, *Appl. Catal. B: Environ.,* 2006, **63,** 15.
27 L. Li, X. Wang, Y. Lan, W. Gu, and S. L. Zhang, *Ind. Eng. Chem. Res.*, 2013, **52,** 9130.
28 J. F. Li, G. Z. Lu , H. F. Li, Y. Q. Wang, Y. Guo and Y. L. Guo, *J. Colloid Interface Sci.,* 2011, **360,** 93.
29 T. Feng, X. D. Wang and G. S. Feng, *Mater. Lett.,* 2013, **100,** 36.
30 S. Deshpande, S. Patil and S. Kuchibhatla, *Appl Phys Lett.,* 2005, **87,**133113.
31 A. Corma and P. Atienzar, *Nat. Mater.,* 2004, **3, 3**94.
32 X. Wang, P. Tian, Y. Lin and L. Li, *J. Alloys Compds.*, 2015, **620**, 228; X. Wang, F. Gu, L. Li, G. Fang and X. Wang, *Mater. Res. Bull.*, 2013, **48**, 3761.
33 X. Wang, Y. Lin, X. F. Ding and J. G. Jiang, *J. Alloys Compds.*, 2011, **509**, 6585.
34 Z. Wang, G. L. Shen, J. Q. Li, H. D. Liu, Q. Wang and Y. F. Chen, *Appl. Catal. B: Environ.,* 2013, **138-139**, 253 ; X. Wang, H. M. Mao and Y. C. Shan, *RSC Adv.*, 2014, **4 (67)**, 35614.
35 L. W. Qian, J. Zhu, W. M. Du and X. F. Qian, *Mater. Chem. Phys.,* 2009, **115,** 835.
36 A. H. Morhed, M. E. Moussa, S. M. Bedair, R. Leonard, S. X. Liu and N. A. El-Masry, *Appl. Plys. Lett.*, 1997, **75**, 2389.
37 S. Maensiri, C. Masingboon, P. Laokul, W. Jareonboon, V. Promarak, P. L. Anderson and S. Seraphin, *Cryst. Growth Design*, 2007, **7**, 950.
38 F. M. Meng, L. N. Wang and J. B. Cui, *J. Alloys Compd.*, 2013, **556**, 102.
39 S. G. Wu, L. Z. Zheng, L, Rui and X. Q. Lin, *Electroanalysis*, 2001, **13**, 967.
40 Ch. Comninellis, *Electrochim. Acta*, 1994, **39**, 1857.
41 Y. Liu, H. L. Liu and Y. Li, *Appl. Catal.,B: Environ.*, 2008, **84**, 297; Q. Z. Dai, L. C. Lei and X. W. Zhang, *Sep. Purif.Technol.,* 2008, **61**, 123.